



Characterization of the mechanical properties and microstructural evolution of martensitic steel in repeated tempering cycles

Amitkumar Shelar, B. P. Ronge

Sveri's College of Engineering, Pandharpur, University of Solapur, India
amitkumarshelar@gmail.com, <http://orcid.org/0000-0002-0006-8094>
bpronge@coe.sveri.ac.in

ABSTRACT. The purpose of this study was to understand the behavior of martensitic H13 steel in accordance with the microstructural evolution, mechanical properties and wear in repeated tempering cycles. The microstructures were characterized by an axio image observer microscope, scanning electron microscope (SEM), and x-ray diffraction (XRD). Uniaxial tensile test, Charpy v-notch impact test, rockwell hardness test and wear test were conducted to analyze the changes in mechanical properties, impact properties, hardness and wear in repeated tempering cycles. The specimens prepared were subjected to hardening at 1030 °C for 20 minutes, oil quenched and subjected to repeated tempering cycles at 570 °C for 2hrs holding time each. The mechanical properties recorded indicate that the maximum ultimate tensile strength obtained was at double tempering due to secondary hardening effect i.e., alloy carbides precipitation offering strength to the matrix and corresponding wear was found to be minimum. The annealed specimen revealed bainitic microstructure and with hardening and repeated tempering cycles, fine needle like structure and carbides were observed in the microstructure and retained austenite was converted into martensite and martensite was converted into tempered martensite. Carbide size and martensite lath distribution control the strength.

KEYWORDS. Heat treatment, Mechanical Properties, Microstructure evolution, Fractography, Wear.



Citation: Shelar, A., Ronge, B. P., Characterization of the mechanical properties and microstructural evolution of martensitic steel in repeated tempering cycles, *Frattura ed Integrità Strutturale*, 66 (2023) 38-55.

Received: 26.05.2023
Accepted: 09.07.2023
Online first: 19.07.2023
Published: 01.10.2023

Copyright: © 2023 This is an open access article under the terms of the CC-BY 4.0, which permits unrestricted use, distribution, and reproduction in any medium, provided the original author and source are credited.

INTRODUCTION

H13 hot work die steel material shows superior properties at elevated temperatures. H13 steel possesses high working hardness, better corrosion resistant properties, wear resistant properties and hot toughness. With the plastic deformation there is stress concentration in large carbides which increases crack initiation and coarse carbides propagates cracks [1]. In numerous studies, the hardening and tempering effect on the H13 steel was analyzed and the specimens were tested for different austenitizing range around 980°C to 1040°C and different tempering



temperature range around 550 °C to 650 °C. The excellent mechanical properties for H13 tool steel were obtained after austenitizing at 1040°C and at tempering temperature 570°C with uniform microstructure [2-5]. As in the temperature range 100-200°C there is formation of ϵ Epsilon carbides and in 200-350°C temperature range there is the transformation of retained austenite into a mixture of ferrite and cementite, transition carbides are replaced by cementite decreasing toughness due to which tempering temperature above 500°C is preferred as the martensite lath boundaries are stable in the temperature range of 500-600°C [6].

H13 steel contains chromium, molybdenum and vanadium as the major contributing elements in the composition. After hardening and tempering of H13 steel, the carbon combines with V, Mo, and Cr to form V rich MC type carbides, Cr rich Cr_7C_3 carbides and Mo rich M_2C type of carbides. The vanadium-based carbides and molybdenum-based carbides promote high temper stability in steel by reducing the forming of carbides at the grain boundaries which reduces the austenite at the carburized layer and thus contributes to the improvement in wear resistance [7]. H13 steel with chromium content 5% and modified steel with reduced chromium to 3% were compared, it was observed that beyond 600°C tempering temperature and 2 + 2hr holding time the carbides precipitation was suppressed and at 600°C tempering temperature and 2 + 2hr holding time in 5% Cr H13 steel the carbide mainly formed was Cr_7C_3 distributed along the grain boundaries and lath boundaries, whereas with reduced 3% Cr steel the vanadium carbides were formed with short structure and it was observed that with reducing Cr content the temper stability and high temperature strength was improved [8].

With the increase in quenching temperature from 800 to 900°C for the medium carbon low alloy steel and the composition equivalent to 4340 steel, the tensile strength increases due to the strengthening of the grain boundaries and solid solution strengthening of the dissolved carbides, whereas with the increasing tempering temperature from 550°C to 650°C the tensile strength found to be decreasing mainly due to dislocation strengthening mechanism and long chain carbides formation [9]. Mo, V promotes the temper stability of steel and vanadium carbides precipitates formed in the tungsten modified die steel during tempering is responsible for delaying softening of martensite due to causing difficulty in movement of dislocations whereas tungsten has less ability to form carbides when compared with molybdenum and vanadium [7]. With the increase in vanadium from 0 to 0.3% in 718H pre-hardened mold steel, MC types of carbides increases which contributes to the precipitation strengthening mechanism and grained boundaries were pinned and mobility was decreased affecting toughness [10].

The wear rate depends on the hardness and fracture stability of H13 steel. Wei et al. [11] performed the wear test for tempered specimens from 200°C to 700°C temperature range, up till 600°C better wear resistance was shown but thereafter wear resistance decreases in the case of H13 steel. Barrau et al. interpreted that the abrasion resistance depends on size, density of carbides and dislocation density [12]. Bahrami et al. studied that at high load i.e., 98N the specimens tempered for 30min-60min at 600°C have a high wear rate [13]. Jagota et al. presented that the minimum wear rate was obtained at a tempering temperature of 580 °C and for a tempering time of 1.4hrs [14].

The present study examines the effect of reducing austenitizing soaking time with repeated tempering cycles on H13 steel and investigates the changes in mechanical properties, microstructures, phases, and wear properties during each tempering cycle and some important remarks were put forth by studying the evaluated results. The mechanical properties were found to be improved after double tempering with the corresponding minimum wear.

MATERIALS AND METHODS

The composition of the material of Cr-Mo-V steel was confirmed with the spectrometry and the following compositions were noted as mentioned in Table 1. The sixteen specimens with dimensions 25mm diameter x 180mm long were heat treated.

Elements	C%	Si%	Mn%	P %	S%	Cr%	V%	Ni%	Mo%
H13 steel	0.413	1.10	0.384	0.021	0.0089	5.21	0.77	0.272	1.31

Table 1: Chemical composition of the H13 steel (wt.%).

Heat treatment layout

A muffle furnace was used to carry out the heat treatment cycles. The heat treatment cycle was designed based on the earlier study mentioned in the introduction [2-5, 14]. All the specimens were preheated at 650°C and 850°C for 5 minutes,

preheating was done to establish a uniform temperature throughout the specimen before reaching to austenitizing temperature. After preheating, the specimens were heated to the austenitizing temperature at $1030 \pm 10^\circ\text{C}$ for 20 minutes, as at this temperature uniform microstructure is achieved. The austenitizing temperature is an important parameter as it controls the grain size coarsening [2]. Oil quenching was done by using clever brand quench oil, it is necessary, as oil quenching minimizes the capacity of quench distortion. The repeated tempered cycle was performed at $580 \pm 10^\circ\text{C}$ and for 2hrs holding time and in each tempering cycles the performance in terms of changes in mechanical properties and microstructures for hot work steel is reported. During each tempering cycle, the martensitic steel is heated below the eutectoid temperature i.e., below 700°C and air cooled as shown in figure 1.

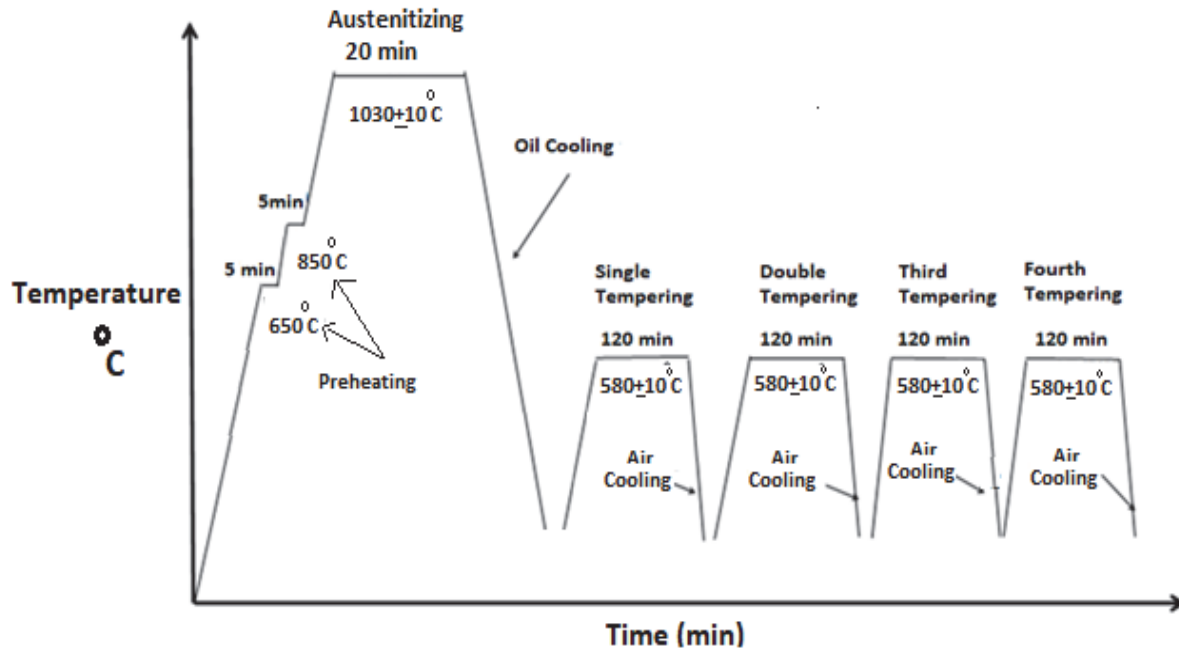


Figure 1: Heat treatment chart.

Sr. No.	Nomenclature for specimen	Holding time in Tempering (minutes)
1.	Untreated H13 steel	--
2.	T1: Hardened + Single Tempering at $580^\circ\text{C}/(2\text{hr})$	120
3.	T2: Hardened + Double Tempering $580^\circ\text{C}/(2+2\text{hr})$	120+120
4.	T3: Hardened + Third Tempering ($580^\circ\text{C}/(2+2+2\text{hr})$)	120+120+120
5.	T4: Hardened + Fourth Tempering $580^\circ\text{C}/(2+2+2+2\text{hr})$	120+120+120+120

Table 2: Heat treated conditions and nomenclature used for the specimen.

Uniaxial test

The uniaxial tensile test was carried out for untreated H13, T1, T2, T3, and T4 specimens prepared as per ASTM A370:2020 standards. The specimen prepared for the tensile test is shown in figure 2 a) and the schematic diagram is shown in figure 2 b). The mechanical properties were evaluated for the different heat-treated conditions by conducting uniaxial tensile tests on 3 samples for each condition and average value was used for analysis as specified in table 4.

Impact and Hardness tests

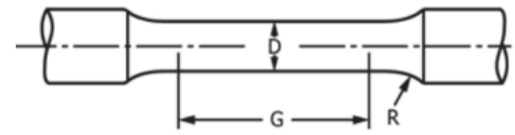
The set of 3 specimens for impact tests were prepared for each heat treated condition as per Charpy v-notch specifications with dimensions $10 \times 10 \times 55\text{mm}$. The impact test was carried out on IT-30 (ASTM) Charpy impact testing machine to evaluate the impact energy absorbed by the specimens at each tempering condition. The specimen prepared



for carrying out the Charpy impact test are shown in figure 2 c) and d) for all tempered conditions. The hardness values were recorded by using a Rockwell Hardness tester.



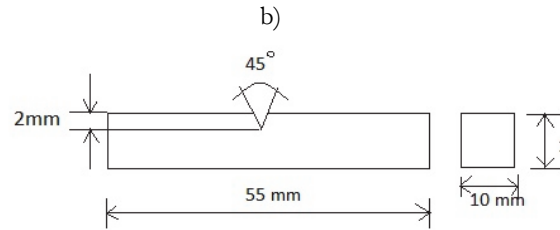
a)



G - Gauge length - 50mm, D - Diameter - 12.5mm, R - 10mm



c)



d)



e)



f)



Pin on Disk Wear Testing Machine

g)

Figure 2: a) Specimen prepared for tensile test b) Schematic diagram c) Specimen prepared for Charpy impact test d) Schematic diagram of specimen for Charpy impact test e) Specimen for optical and SEM f) Specimen for fractography g) Wear test setup

Microstructure analysis

The microstructures were prepared as per ASTM E3:2017/ASTM E-407-07e1(RA2015)/ASM handbook Vol. 9. The annealed specimen was treated with 2% villeda's reagent and the other specimens were treated with 2% nital reagent. The specimen prepared was as shown in figure 2 e). The microstructures for all the specimens under different heat treatment conditions were observed by using an axio image observer to find the changes in the microstructures formed as well as the surface morphology was characterized by FE-SEM and point EDS was done to find the distribution of elements and to get a clearer interpretation of changes in the microstructure. The microstructure of the specimen was characterized by X-ray diffraction (XRD) using cobalt radiation (Co-K α) as a source with a step size of 0.002 $^\circ$ and phase angle considered

Sr. No.	Parameter	Values
1	Disc	EN32
2	Load	100N
3	Sliding Distance	2400m
4	Velocity	2m/sec
5	Hardness of Disc	62 HRC

Table 3: Parameters for pin-disc test.



from 20° to 110°. The XRD data, including the peaks, phase angle, dislocation density, micro-strain, full-width at half maximum (FWHM), and integral strength of the diffraction peaks were analyzed using Xpert highscore software. The fractography results were observed using scanning electron microscope (SEM) for different tempering conditions to analyze the type of fracture formed in the tensile test.

Wear test

The wear test was performed to evaluate the coefficient of friction and wear variation with repeated tempering cycles. Figure 2 e) shows the pin disc wear setup for performing the wear test and table 3 shows the specifications and parameters used for performing the wear test. The wear test setup used was originally from ducom instruments.

RESULTS AND DISCUSSION

Mechanical properties analysis

The mechanical properties changes were evaluated in each tempering cycle and are mentioned in table 4.

Sr. No.	Parameters	Untreated H13 Steel	T1	T2	T3	T4
1	Yield Strength (MPa)	350.05	952	945	907	870
	Standard deviation	± 20.1	± 2	± 3.51	± 6.357	± 10
2	Ultimate Tensile Strength (MPa)	641.32	1122	1165	1116	1081
	Standard deviation	± 30.02	± 9.615	± 13.229	± 11.59	± 19.51
3	% Elongation	31.80	11.48	12.40	12.58	14.40
	Standard deviation	± 9	± 0.52	± 1.2	± 0.99	± 1.253
4	Reduction of Area (%)	66.72	22.31	19.32	24.80	25.49
	Standard deviation	± 4	± 3.2327	± 1.9	± 1.9	± 2.134

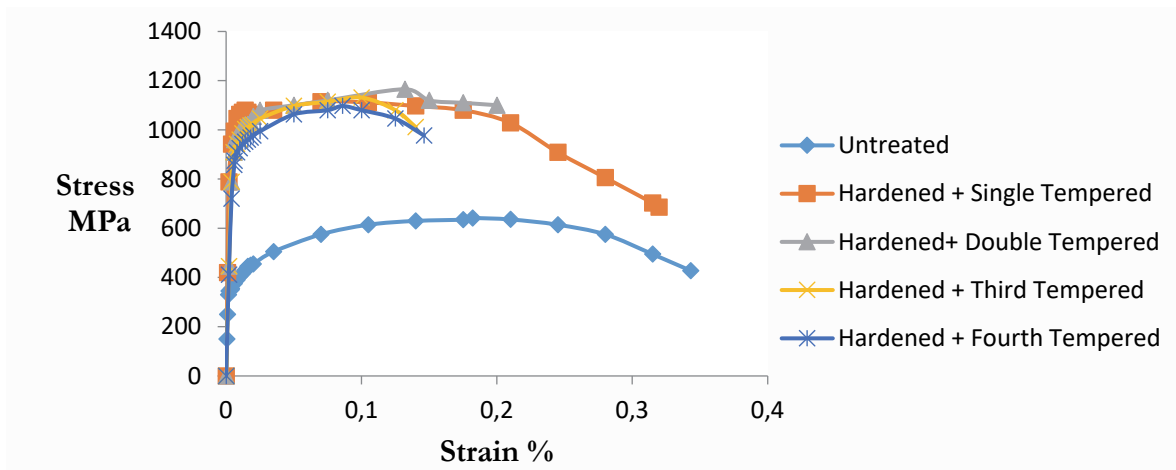
Table 4: Mechanical properties of specimen at different heat-treated conditions

Uniaxial Test

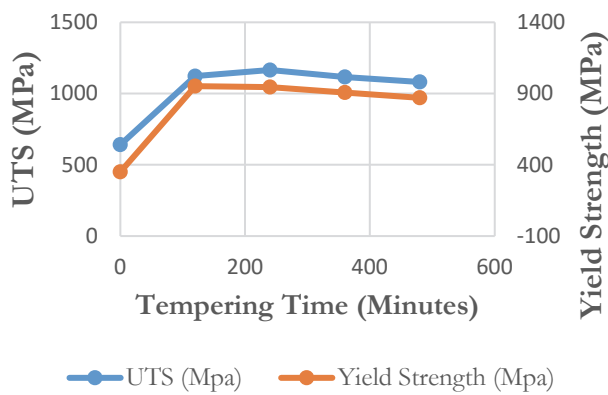
The recorded value of yield strength indicates a decreasing trend and from single tempering to double tempering the drop in yield strength is negligible i.e. from 952Mpa to 945Mpa indicating that there is no much change in yield strength when there is a transformation from elastic to plastic behavior whereas ultimate tensile strength value increases from single to double tempering i.e. from 1122Mpa to 1165Mpa which indicates an increase in strength due to secondary hardening i.e. due to precipitation of alloy carbides. It can be clearly stated from the results evaluated that with the lowered soaking period during hardening, there is decrease in ultimate tensile strength when compared with the results reported by the researchers, though the secondary hardening phenomenon contributes to a rise in ultimate tensile strength by 3.8% which can be attributed to the formation of MC type of vanadium rich carbides favouring the strengthening mechanism [10]. It was also observed that during repeated tempering cycles the change in ultimate tensile strength ranges from 3% to 5% and for the yield strength after double tempering the change is around 4% when the soaking time for hardening is reduced. The properties obtained were inferior when compared with the standard data specified by NADCA standards which can be due to partially dissolved carbides because of a reduced soaking period or due to decarburization as atmospheric conditions were not controlled. In repeated tempering cycles, the ultimate tensile strength increases after double tempering and thereafter decreases whereas the hardness drops significantly which can be due to the tempering of the specimens around 580°C, as above 550°C secondary hardening effect decreases due to breaking of coherence and coarsening of carbide particles as reported by Qamar et al. [18].



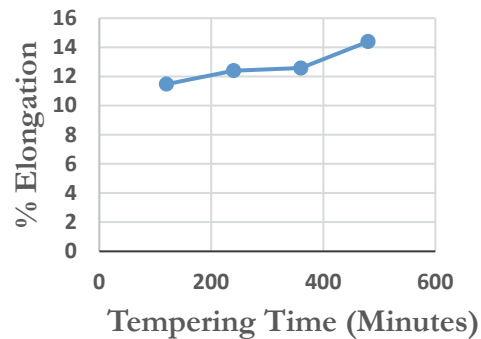
The stress strain curve showed in figure 3 a) was plotted from the raw data recorded for single specimen for all heat treated conditions which shows combination of readings with the use of extensometer till yield (up to 1.6%) and after removal of extensometer to avoid damage of extensometer the readings recorded were from grip-grip to consideration which shows more strain than actual strain. The results obtained were compared with the results obtained by Wang et al. [2] for the same heat-treated boundary conditions of H13 steel having composition C 0.39%, Cr 5.09%, Mo 1.45%, V 0.92%, Si 1.04%, Mn 0.4%, the ultimate tensile strength was found to be lowered by around 62.65% whereas % elongation was increased by around 78.22%. The comparison was done with the minor difference in the composition as well as the heat treatment furnace used was a vacuum furnace by the researcher. So, it can be concluded that with the lowered austenitizing soaking time to 20min the ultimate tensile strength decreases but % elongation increases though this is a rough interpretation as there is slight alteration in other element composition within a specified range of AISI standards of H13 steel and the heat treatment was done in vacuum furnace as in this case muffle furnace was used for the heat treatment with different soaking and quenching condition. The results obtained were again compared with the H13 steel double tempered at 650°C (elements were within range as per AISI standards) and it was observed that the ultimate tensile strength was found 18.45% more in H13 steel in the present case [15].



a)



b)



c)

Figure 3: a) Stress vs. Strain curve plotted with consideration of values of extensometer till yield and beyond that grip to grip consideration for all heat-treated conditions. b) Ultimate tensile strength vs. Tempering Time and Yield Strength vs. Tempering Time c) % Elongation vs. Tempering Time

The % elongation increased from 11.48% to 14.40% indicating ductility increases with the increasing tempering cycles. The mechanical properties and microstructures were refined with the increase in tempering temperature [16]. It is discussed in the later part incorporating microstructural changes with the change in mechanical properties.

Effect of repeated tempering cycles on hardness and impact toughness

The austenite decomposition and precipitation of carbides during tempering improve the toughness by relieving the residual stress [3]. The strength of the matrix contributes for improving the hardness, reducing the volume fraction of retained austenite in martensitic steel increases the strength of the steel [17], it can be correlated with the mechanical properties obtained indicating increasing ultimate tensile strength initially. With the repeated tempering cycles, the hardness drops from 46HRC to 38HRC and Charpy impact test indicates the variation of impact energy within a narrow range, it might be due to the partial dissolution of carbides which lowers the carbides precipitation and thus there is a drop in interfacial energy [10] as indicated in table 5 and behaviour is plotted in figure 4 a) and b). The results obtained were inferior when compared with the results obtained by Guanghai et al. [3], it can be due to the partial dissolution of carbides due to the insufficient soaking period during austenitizing resulting less amount of carbides precipitation which affects the ultimate tensile strength, lowers the hardness and yield strength, as intermediate products like bainite formed will create hard spots and acts as stress raiser and there is increase in % elongation indicating material becomes softer and ductile with the repeated tempering cycles.

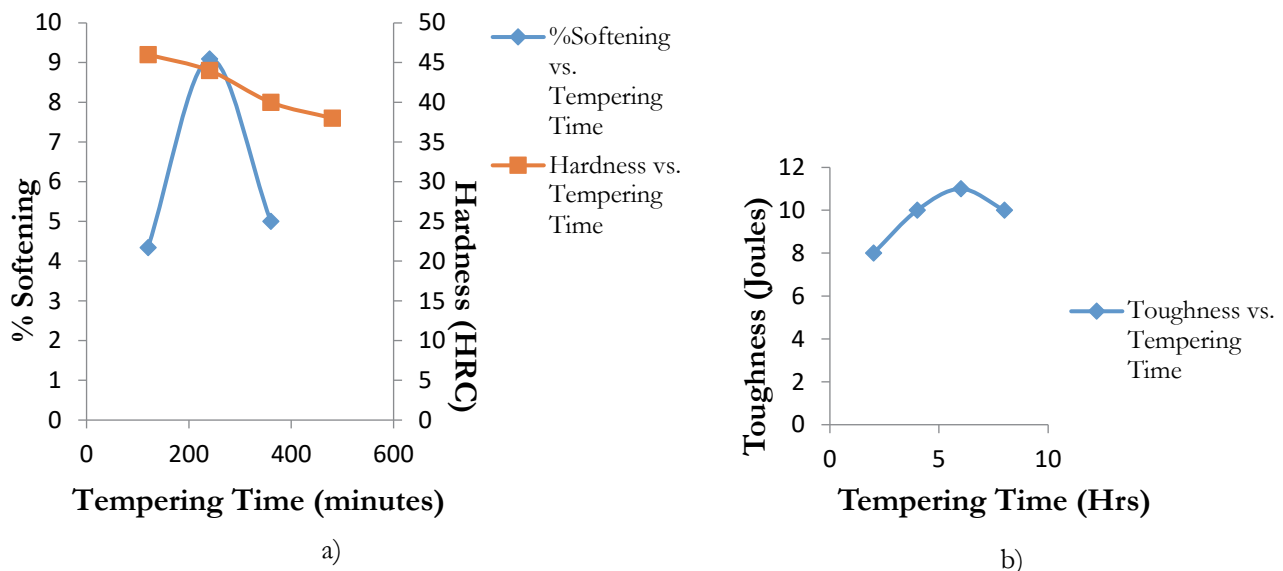


Figure 4 a) % Softening, Hardness (HRC) vs. tempering time b) Toughness vs., tempering time (minutes)

% Softening can be calculated as [33]:

$$\% \text{ Softening} = \frac{(\text{Initial hardness} - \text{final hardness})}{\text{Initial hardness}} \times 100 \quad (1)$$

Parameter	T1	T2	T3	T4
%Softening	-	4.34	9.09	5.00
Hardness (HRC)	46	44	40	38
Energy Absorbed (Joules)	8	10	11	10

Table 5: Hardness and toughness for different tempering conditions.

% Softening calculated using eq. 1 increases with the increasing tempering time which shows the increase in % ductility which can be observed in table 5. With the conversion of retained austenite to martensite there are chances of developing compressive stress which suppresses crack growth [19]. Grain refinement plays a significant role to resist cleavage failure by providing a barrier to crack propagation [20]. V is responsible for grain refinement in medium content Cr, Mo, V, steel and Cr and Mo is responsible for grain coarsening in higher content Cr, Mo, V steel [21].



Effect on Strain hardening exponent

One of the important reasons behind improving ultimate tensile strength properties can be specified in a way that after first tempering there is strain hardening phenomena, which is due to dislocation density and dispersion of Fe-C coarse carbides into fine alloy carbides and later on it gets converted into chromium carbides [32]. At hardening and single tempering, the value of strain hardening exponent was 0.071 and at double tempering, it reaches to peak of around 0.11 and thereafter it drops proportionally as shown in figure 5. From the curve it can be calculated and stated that the strain hardening exponent varies within a range from 0.071 – 0.11 in repeated tempering cycles as mentioned in table 6. Normally, dislocation density weakens the crystal but in the case of hot work steel, due to interaction between dislocations and interference of dislocation with the other dislocation causes difficulty in motion. The dislocation density values evaluated are mentioned in table 7. The Holloman flow curve equation (2) defines the relationship between true stress and true strain, whereas n is the strain hardening exponent and the strength coefficient K is calculated and mentioned in table 6.

$$\sigma_T = K \epsilon_T^n \tag{2}$$

σ_T = True Stress

ϵ_T = True Strain

K = Strength Constant

n = Strain hardening exponent

Specimen	Tempering Time (min)	Strain hardening exponent (n)	Strength Coefficient (K)
Untreated H13	--	0.18	1043.63
T1	120	0.072435	1467.04
T2	240	0.1142	1676.82
T3	360	0.04033	1340.26
T4	480	0.04199	1305.58

Table 6: Strain hardening exponent under different heat treatment conditions.

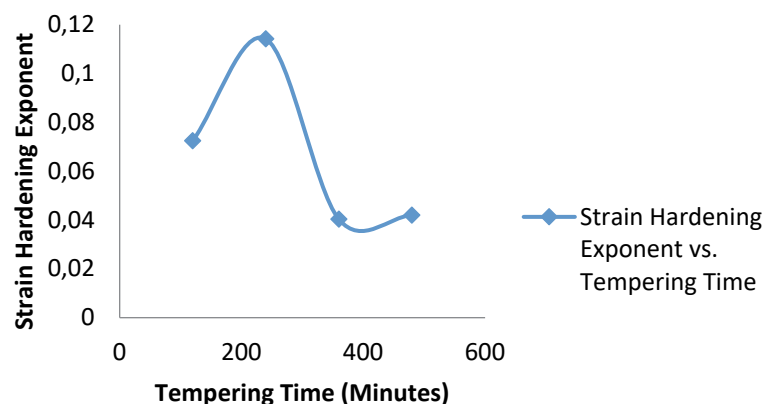


Figure 5: Effect of Strain Hardening Exponent



MICROSTRUCTURE STUDY

Microstructure observation

The microstructures were observed for all the tempering heat-treated conditions (grain boundaries are marked with yellow dotted lines) by using an axio observer microscope with 500x magnification and the images captured are shown in figure 6 a) b) c) d) e).

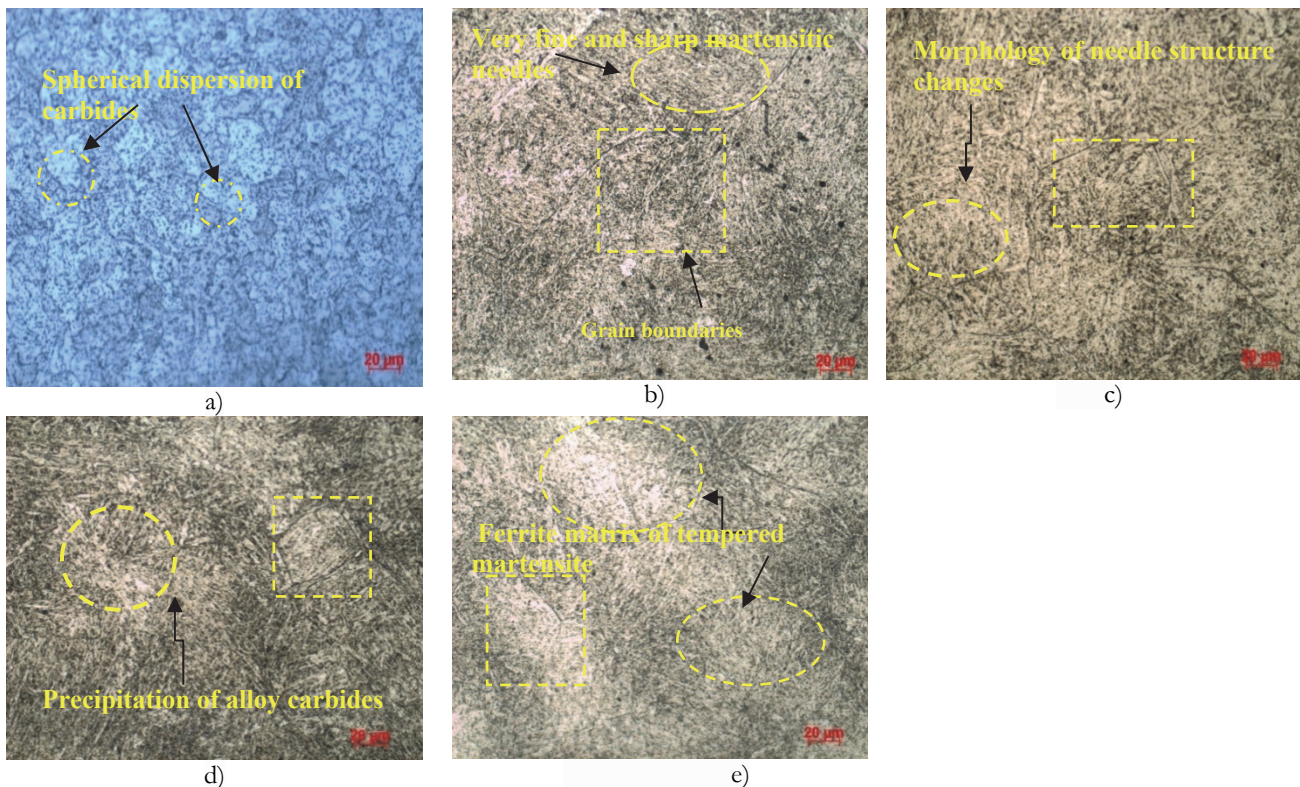


Figure 6: Microstructure analysis a) Untreated H13 b) Hardening + Single Tempered c) Hardening + Double Tempered d) Hardening + Third Tempered e) Hardening + Fourth Tempered.

The microstructure of untreated H13 steel in annealed condition shows a bainite structure with coarse carbides as observed in figure 6 a) and in repeated tempering cycles, the tempered martensite and fine needle like structure was observed. When the microstructure formed is correlated with the mechanical properties as shown in table 4, it can be stated that due to coarser grain size, there are fewer grain boundaries (which can be observed more clearly in the later part of SEM images) and mechanical properties (ultimate tensile strength) found to be low and elongation found to be increased. As quenched microstructure contains carbon in supersaturated form and with the repeated tempering cycles the carbon reacts with Cr, Mo, V and Cr rich, Mo rich, V rich carbides were formed. After double tempering in figure 6 c) needle like structure of tempered martensite can be observed which is formed as a result of a slip or twinning action in the internal structure.

With the repeated tempering cycles from figure 6 b) to 6 e) and the SEM images shown in figure 7 a) indicate that the needle like structure gets shortened and the morphology of the needle changes as the stresses are relieved and the retained austenite present is converted into martensite and martensite is converted into tempered martensite. When quenched and tempered, the alloy carbides precipitate and when carbon combines with Fe in the form of cementite, the complete relief of carbon present in the supersaturation form in the martensitic matrix is achieved. In figure 6 e) the grain boundaries are properly visible, and increased carbide formation with the increase in the ferrite matrix can be observed.

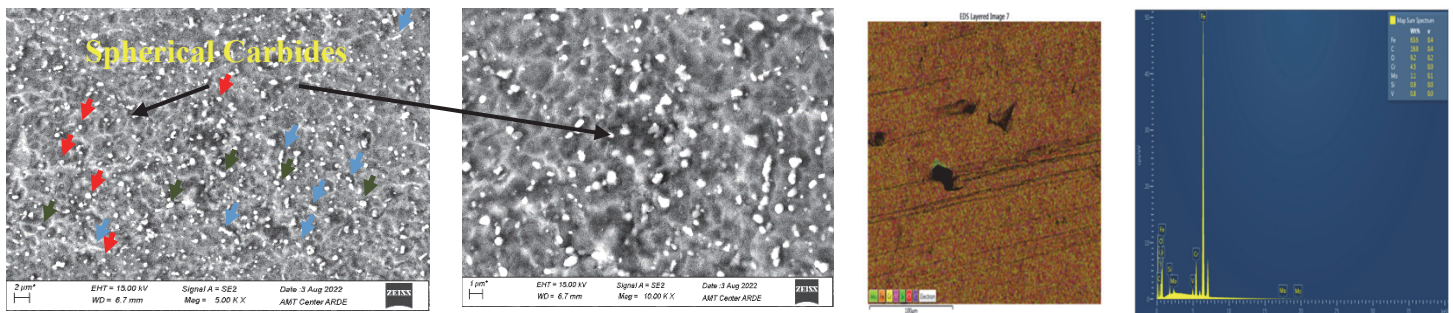
Surface morphology analysis

The microstructure was observed under scanning electron microscope for as received condition and for repeated tempering conditions. The Energy Dispersive Spectroscopy (EDS) was taken at point for chemical characterization of

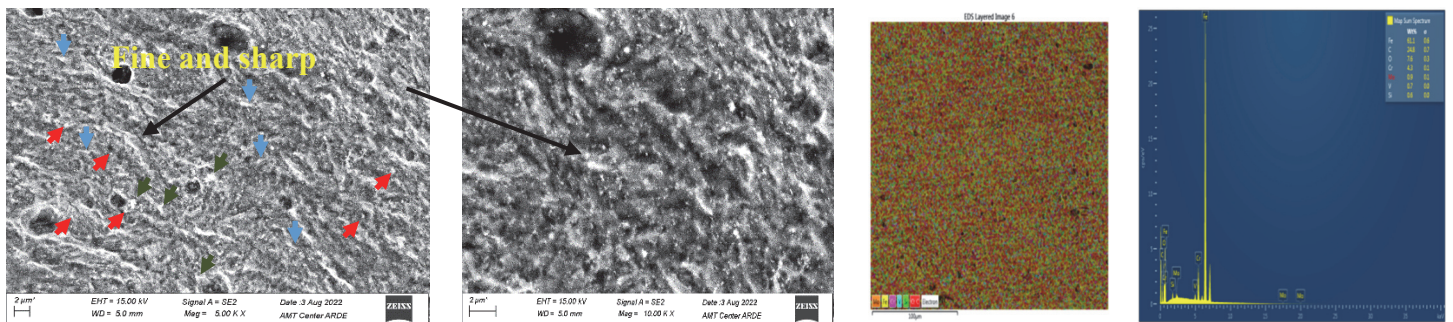


material i.e., measuring atomic mass and wt. % of elements for repeated tempering conditions. With the repeated tempering cycles, the morphology and martensite lath structures appear to be changing as observed in figure 7 a). The needle shape structure appearing indicate M2C type of Mo-rich carbides [22] and it varies in the range 5-6.5 μ m. In triple tempering condition, the lath width increases as mentioned in table 7 and sharpness decreases as shown in figure 7 b) which indicate stress is relieved. With the relieving stress, there is increase in precipitation of cementite which is present in the form of globular structure and further it gets converted into stable M23C6 carbides to produce a bcc ferrite matrix of tempered martensite. The sequence of carbides precipitation during tempering for steel with chromium is - Matrix \rightarrow M3C \rightarrow M7C3 \rightarrow M23C6 and with molybdenum is - Fe3C \rightarrow M2C \rightarrow M6C and the presence of Mo as alloying element reduces the coarsening rate of M7C3 as stated by Bhadesia et al. [32].

The % elongation values recorded – For the T1 condition was around 11.48%, for the T2 condition was 12.4%, for the T3 condition was 12.58% nearly the same with respect to T2 and for the T4 condition was 14.4%. From such conditions, it can be concluded that from single tempering to double tempering condition % elongation increases and the morphology observed is martensite lath, in double and third tempering % elongation is nearly same which indicate that further carbide precipitates without much change in ductility and with the further tempering the width of the martensite laths increases as stresses are getting relieved and the %elongation increasing indicating material becomes softer. Thus, it can be interpreted that the alloying element present in tool steel precipitates in the form of carbides i.e., secondary carbides present precipitates and increases the strength of the matrix in double tempering as indicated in table 4 (the value of ultimate tensile strength) without affecting ductility much in third tempering. Therefore, it can be concluded that the lath martensite morphology formed could be the reason to increase the ultimate tensile strength in single and double tempering conditions. Another important observation made after looking at the surface morphology (orientation of laths) and mechanical properties (ultimate tensile strength) is – when the martensite laths are closely arranged it offers more strength as observed in single and double tempering and later on in the third and fourth tempering condition precipitation of carbides is visible as well as tempered martensite increases making the material softer although the reduced soaking time during austenitizing may not lead to complete transformation of higher % of chromium carbides into austenite and there is formation of intermediate product as bainite in fraction of martensite. The EDS analysis shows uniform distribution of carbides.



Untreated H13 Steel



Hardened + Single Tempering (T1)

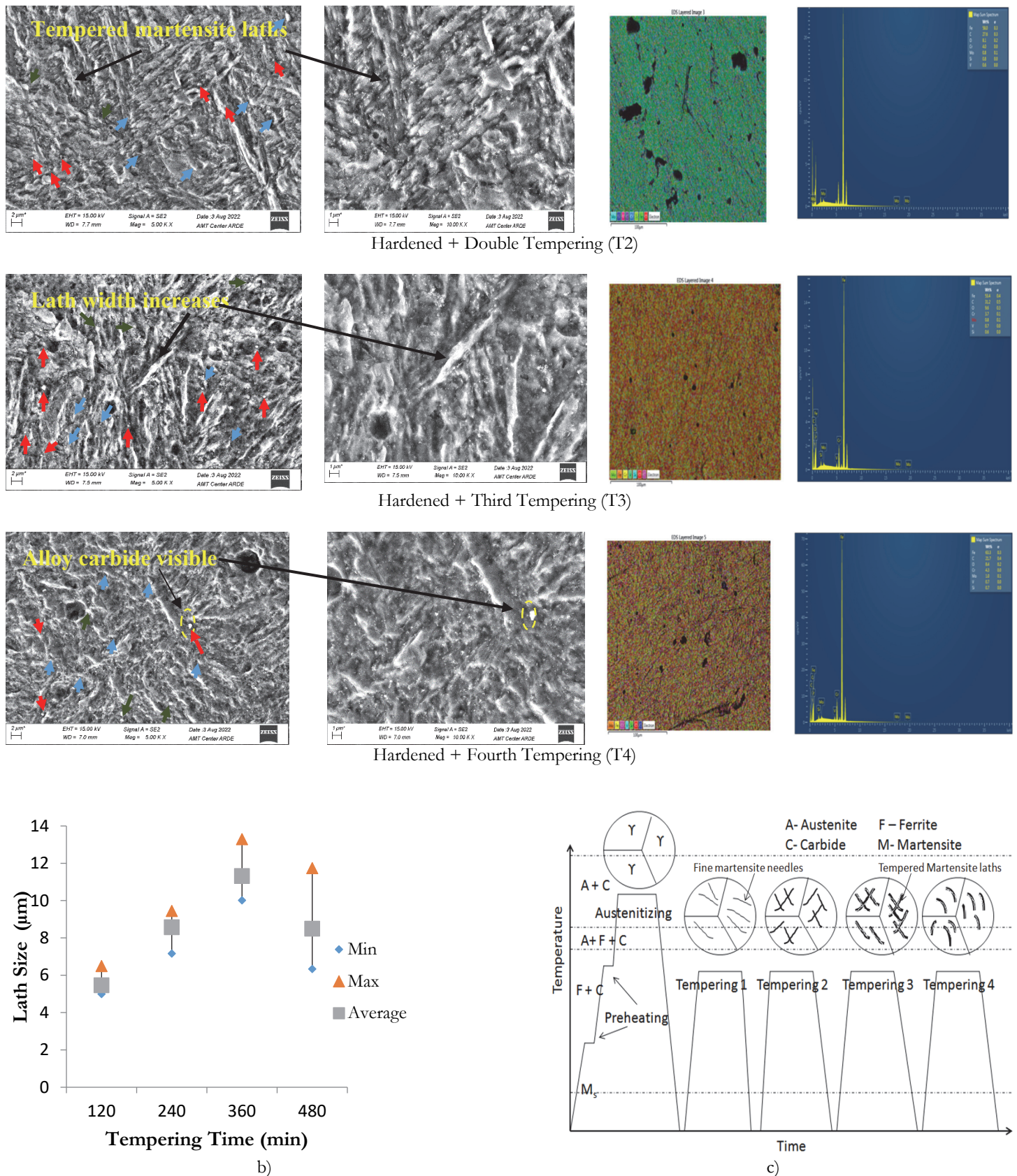


Figure 7: a) Surface morphology and EDS of specimen of Untreated H13 steel, T1, T2, T3, T4 b) Variation of Lath size vs. tempering time c) Change in phases during each tempering cycle.



Sr. No.	Tempering conditions (hrs)	Lath Length (μm)	Lath width (μm)
1	2	5-6.5	0.34-0.88
2	4	7.1-9.4	0.5-1.0
3	6	10.0-13.3	0.9-1.4
4	8	6.3-11.7	0.73-0.81

Table 7: Comparison of lath length and width with tempering conditions.

The rough interpretation of the changes in the morphology of martensite during tempering cycles is shown in figure 7 c) in which at first tempering, sharp and fine martensite laths are present indicating brittle behaviour of the material. With the repeated tempering cycles, the material starts losing its brittleness and becomes soft as martensite is getting converted into tempered martensite, retained austenite is also getting converted into martensite as well as the width of the laths increases which indicates stresses formed after quenching are getting relieved and mobility of the atoms make the structure stable at high tempering temperature. Interlath and intralath precipitation of the carbides can be observed from the SEM images presented in figure 7 a) in T3 and T4 conditions.

Carbide size analysis

The untreated H13 hot work die steel consists of V, Mo, and Cr as alloying elements, so during tempering cycles carbon trapped during quenching will try to escape and will react with the alloying elements to form V-rich, Mo-rich and Cr-rich carbides as found from EDS data. The types of carbide morphology observed in the matrix at 200nm scale are shown in figure 7d). The morphologies identified were like fine strip shapes indicated by blue arrows, spherical shapes indicated by red arrows and ellipsoid shapes indicated by brown arrows as represented in figure 7 a) and figure 7 d). The strip shape or rod like carbides and elliptical shape or coarse shape indicated by the brown arrow are chromium rich M7C3 carbides and M23C6 carbides as presented in the literature, the chromium diffuses at the grain boundaries very rapidly so the grain coarsening is observed with chromium rich M23C6 carbides [23]. The fine spherical shape or square type indicated by the red arrow symbolizes vanadium rich MC type carbides as described in the literature [24-27] and typically it varies from 130nm to 170nm.

The carbide size for repeated tempering cycles was analyzed and obtained values are presented in table 8 which indicates that as the tempering time varies from 2hr to 8hr the carbide coarsening occurs along the grain boundaries and as well as gets precipitated inside the laths of the martensite as shown in figure 7 a) and c). If the further tempering is increased from 16hr to 24hr the M23C6 carbide exists and M6C carbide was found at 24hrs in quenched dievar steel with vanadium around 1% [28].

Sr. No.	Carbide size (nm)	% Vol. fraction
Untreated H13 Steel	557.69(217.571-883.719)	70.311
T1	271.96 (177.383-388.723)	32.996
T2	180.23 (133-304.945)	46.279
T3	198.82 (119.609-389.744)	69.013
T4	276.04 (175.262-346.026)	69.682

Table 8: Carbide size analysis.

With the repeated tempering cycles the spherical type of fine carbides decreases and are getting merged into a coarser shape, it can be attributed to Ostwald ripening phenomenon. The coarsening of carbides leads to decrease in the strengthening effect [31]. Through EDS, it was clear that Cr rich M23C6 type of carbides, V rich MC type of carbides and Mo rich M2C type of carbides were found in the microstructure and the same was confirmed by Ning et al. [24] and with the calculation done it was concluded that ESR (Electroslag Remelting) adjusting the thermo-mechanical process control the precipitates and can give optimized steel properties.

The observations drawn from the specimens were based on the mechanical properties and microstructures can be concluded in a way that in the third tempering and fourth tempering conditions the mechanical properties declines and

the microstructure shows coarsening of carbides. Thus, it can be stated that the critical radius for the different alloy carbides and closely distributed parallel orientation of martensite lath in double tempering with a reduced % of retained austenite gives optimum mechanical properties. The aging parameter can be studied for getting the optimized critical radius for the carbides which would suggest better heat treatment boundary conditions.

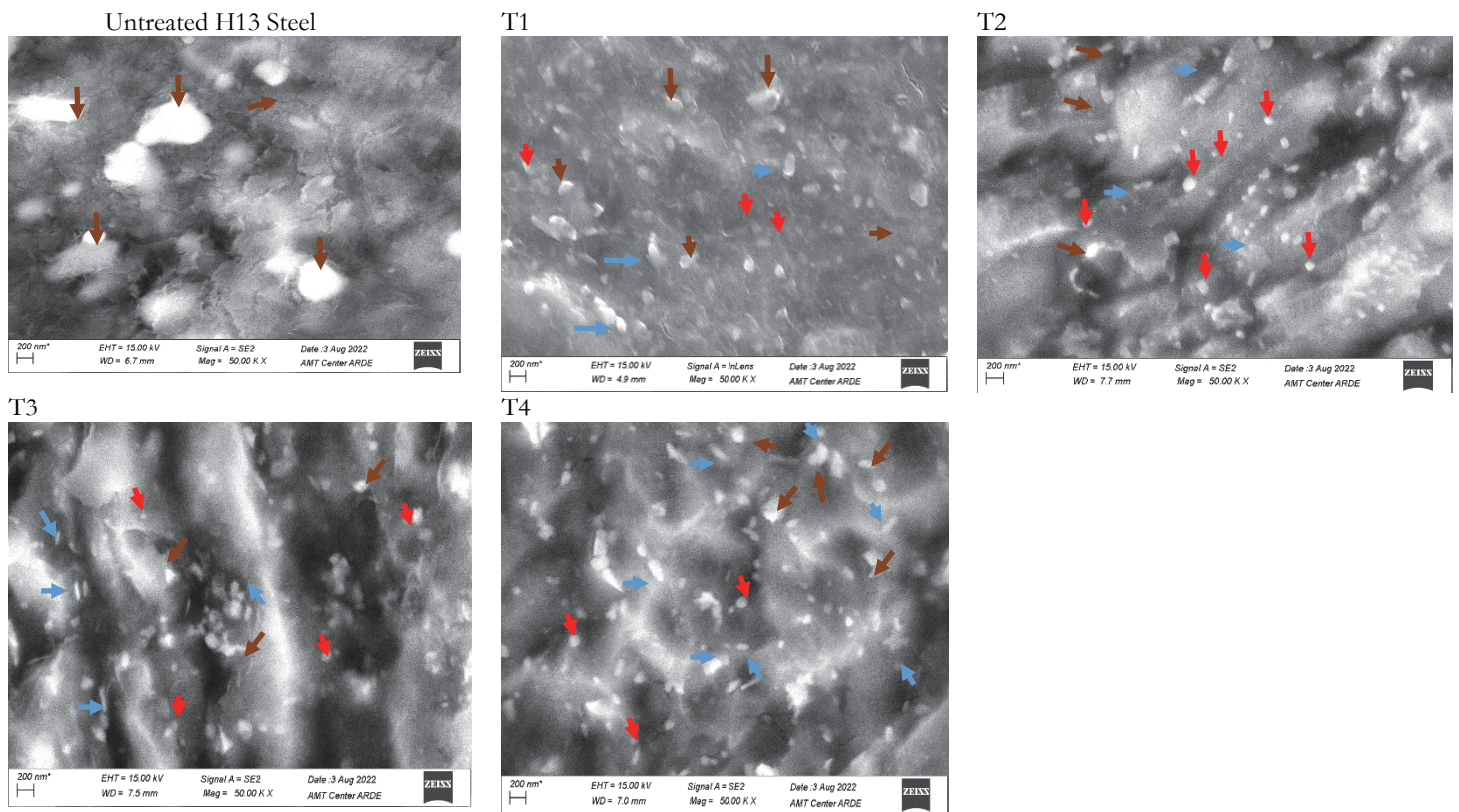


Figure 7: d) Nano-size carbide precipitations at 200nm, morphology observed by SEM Untreated H13 steel, T1, T2, T3, T4

Phase analysis

The XRD plot obtained is shown in figure 8 and the values obtained for microstrain and dislocation density were evaluated by using Xpert highscore software as mentioned in table 9. The values for all the specimens were compared at relative intensity 100% and it was found that dislocation density varies from $4.3825E-05$ to $1.9832E-03$ for the ferrite and the value for microstrain varies in the range $8.47E-5$ to $4.365E-3$. The carbides peak cannot be matched due to less % of alloying elements.

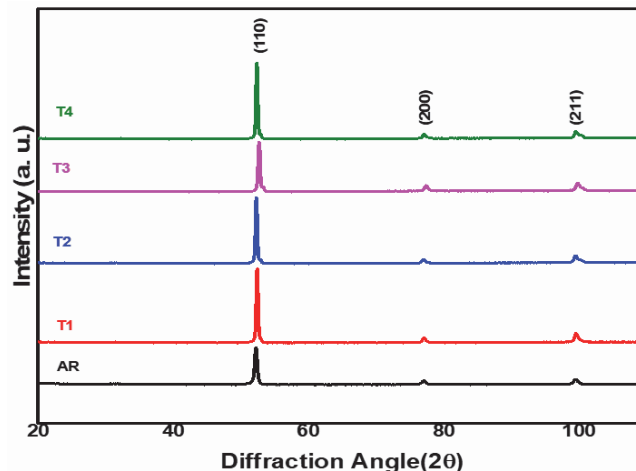


Figure 8: XRD plot for specimen at different tempering conditions.

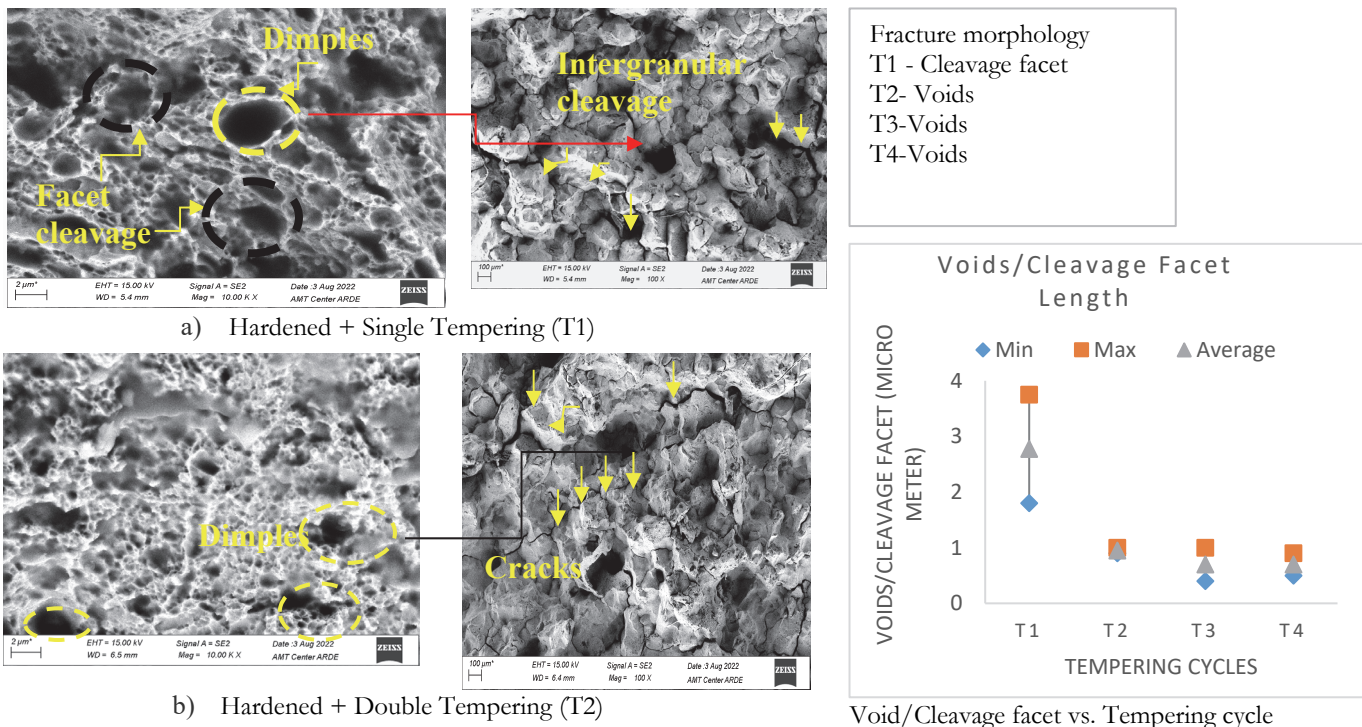
Specimen No.	Pos. [20°]	Θ	Height [cts]	Rel. Int. [%]	FWHM (β)	d-spacing [Å]	Crystallite size (D) [nm]	Dislocation density (δ)	Micro strain (ϵ)
Untreated H13 Steel	52.2095	26.10475	9801.02	100	0.006007867	2.03438	151.05596	4.38252E-05	0.000847
1 (T1)	52.3749	26.18745	19578.09	100	0.035384311	2.0284	22.45510097	0.001983216	0.004365
2(T2)	52.2656	26.1328	17431.06	100	0.0051496	2.03235	168.9191349	3.505E-05	0.000696
3(T3)	52.6857	26.34285	13226.79	100	0.006007867	1.73736	94.58196818	0.0001118	0.00053
4(T4)	52.3295	26.16475	20068.86	100	0.0051496	2.03004	160.4279921	3.885E-05	0.000661

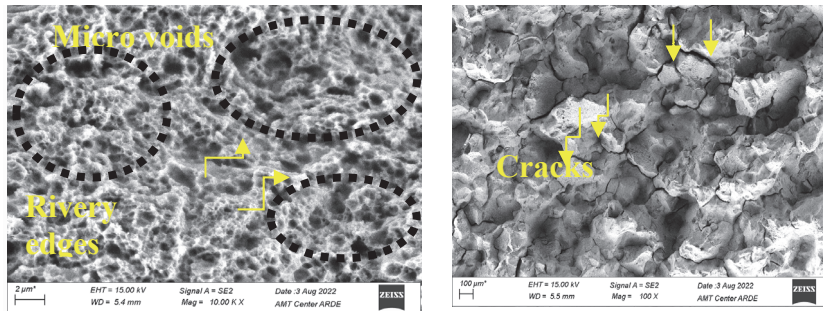
Table 9: Comparison of dislocation density and micro strain for each specimen.

Fractography analysis

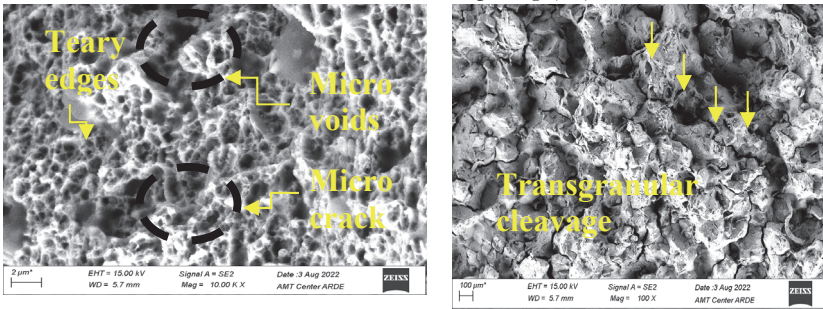
The fractography analysis for tensile test specimens was performed for all heat-treated conditions and the images obtained were shown in figure 10 a), b), c), d). The single equiaxed dimple (yellow mark region) and quasi-cleavage fracture (black marked region) indicating brittle failure with the sign of embrittlement in between the grains was observed in hardening + single tempering condition i.e., in figure 10 a). The dimples were increased in figure 10 b) indicating failure mode shifting from brittle to ductile and in figure 10 c) and d) the various sizes and shapes of dimples distribution with ductile rupture, rivy and teary edges was observed.

It also shows the multiple voids formation as described in table 10 (blacked mark region) and multiple micro cracks with the repeated tempering cycles which propagate and joined by tearing at the surface with the increase in tempering holding time, similar results were observed and presented by Saha et al. [29]. Figure 10 e) presents the distribution of cleavage facets and multiple voids in repeated tempering cycles. Wang et al. [30] studied different high temperature tensile deformation mechanisms and observed its effect on fracture mode formed. It can be concluded that with the lowered soaking period during hardening, the material become softer during repeated tempering cycles as indicated by fractography images with rivy and teary edges as evidence.





c) Hardened + Third Tempering (T3)



d) Hardened + Fourth Tempering (T4)

Morphology observed	Cleavage facet	Voids	Voids	Voids
	T1	T2	T3	T4
Min	1.8	0.9	0.4	0.5
Max	3.75	1	1	0.9
Average	2.775	0.95	0.7	0.7

Table 10. Morphology observations

Figure 10: SEM fractography images for different heat-treated conditions a) Hardening + Single Tempering b) Hardening + Double Tempering c) Hardening + Third Tempering d) Hardening + Fourth tempering e) Void/Cleavage facet vs. Tempering cycle

WEAR TEST

The wear test was conducted on a pin disc wear setup with 100N load, sliding distance 2400m, and sliding speed 2m/sec. The coefficient of friction values with maximum and minimum ranges for all heat-treated conditions is mentioned in table 11. The graphs of the coefficient of friction with respect to time for repeated tempering conditions are shown in figure 11 a).

Sr. No.	Parameter	Untreated H13 steel	T1	T2	T3	T4
1	COF	0.285 (0.25-0.34)	0.194 (0.14-0.26)	0.254 (0.225 – 0.3)	0.225 (0.21-0.24)	0.258 (0.2-0.32)
2	Wear in microns	190	90	85	169	215

Table 11 Coefficient of friction values at different heat-treated condition

With the repeated tempering cycles, it was observed that the coefficient of friction varies in range from 0.26 to 0.32 from single tempering to four times tempering. When wear with respect to sliding distance was evaluated it was observed that the wear varies from 90 micron to 215 micron indicating increase in wear significantly from T2 to T4 as shown in figure 11 b). At T2 condition, the wear was decreased to 85 microns, it can be attributed to the secondary hardening effect i.e., precipitation of alloy carbides increasing strength and offering resistance to wear after double tempering. It is clear from the evaluated results that from double tempering to triple tempering the hardness drops by 9.09% and wear increases by around 98.82% and from third tempering to fourth tempering hardness drops by 5% and wear increases by 27.21%. It can be concluded that after double tempering, the wear rate increases due to coarsening of carbides and drop in hardness.

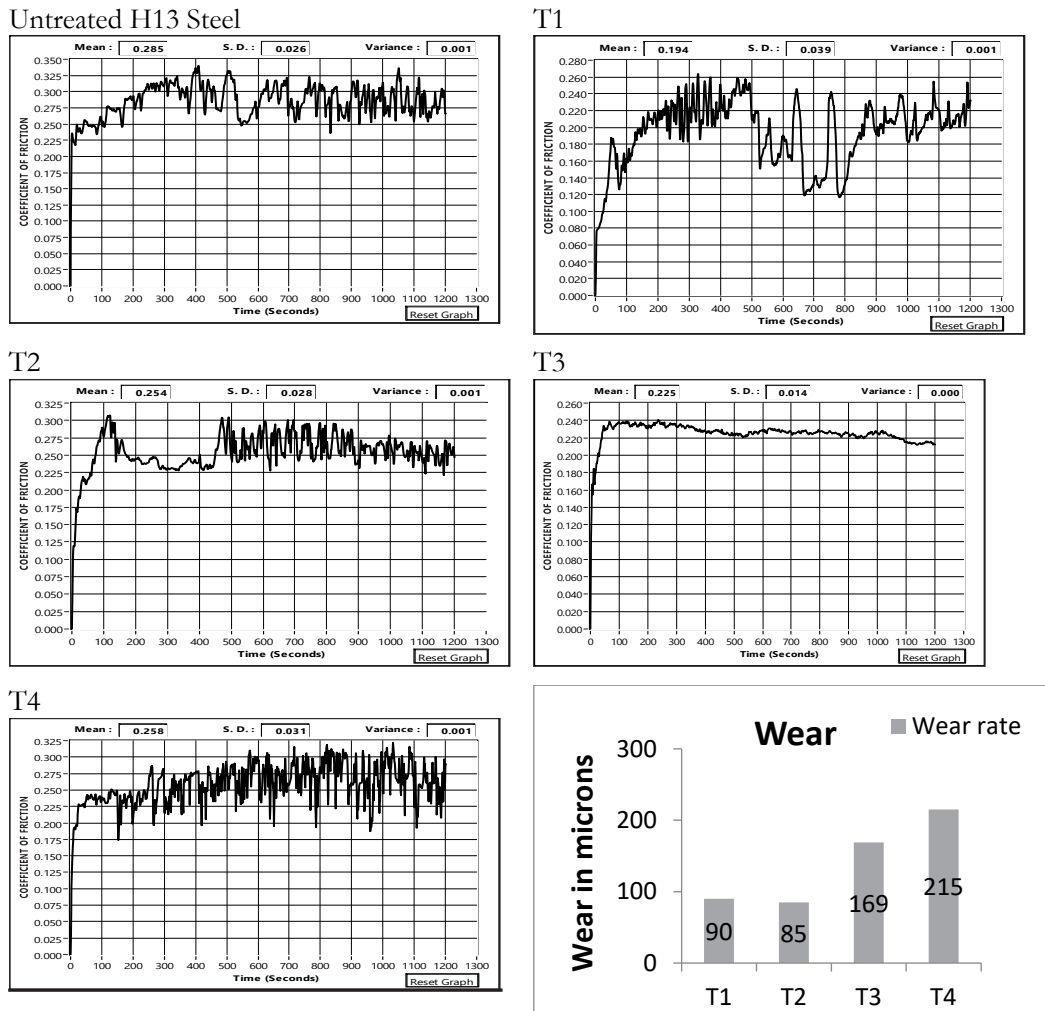


Figure 11 Plot of a) coefficient of friction vs. Time in T1 to T4 b) Wear vs. Tempering cycle

CONCLUSION

In this paper, the effect of repeated tempering cycles on mechanical properties, strain hardening exponent, hardness, impact properties and wear along with the fractography result of the H13 specimen is studied. The main conclusions drawn are as follows:

- It was observed that the reduced soaking time and hardening and double tempering of the specimen give superior mechanical properties (ultimate tensile strength) and thereafter in the third and fourth tempering mechanical properties significantly declined with the minor changes. The % elongation value varies from 11.48% to 14.4% from single to four times tempering condition.
- The critical radius of the carbides, and % volume of fraction increases from double to triple tempering conditions indicating a decrease in mechanical properties, so by controlling the critical radius of the carbides mechanical properties can be controlled. The carbide size varying from 180-272nm and % volume fraction varying from 32.99-46.99% in single-double tempering contributes for better mechanical properties.
- From the morphology of lath martensite formed, it can be concluded that during single and double tempering conditions the closely packed martensite laths orientation controls the strength without affecting ductility. In third and fourth tempering conditions the morphology of the martensite laths width increases which indicates relieving the stresses, closely packed lath seems to get separated as appeared in microstructure resulting softer material.
- The ultimate tensile strength variation in successive tempering cycles is around 3.5%-4.5%. The results evaluated suggest that the double and triple tempering specimens showed nearly the same results along with the relieving of



stresses, so after the third tempering further tempering can be avoided by considering the mechanical properties required for the application.

- The hardness peaks were not observed at 570 °C, thus it can be said that with reduced soaking time at austenitizing, the influence of the secondary hardening phenomenon decreases and above tempering temperature 550°C the hardness peaks are not observed due to breaking of coherence and coarsening of carbides.
- With the increase in tempering time from 120 minutes to 480 minutes, the grains become coarser which decreases the dislocation density and affects the mechanical properties. During single tempering, the mode of fracture was mixed brittle and ductile due to quasi cleavage fracture and dimple observed and the fracture mode was changed from the double tempering condition indicating the ductile fracture due to the formation of dimples, and in further tempering cycles the ductile rupture rivery edges, microvoids, multiple cracks etc. was observed.
- From double tempering to triple tempering, for 9.09% hardness drop there is an increase in wear rate by 98.82% and from third tempering to fourth tempering, for 5% hardness drop wear rate increases by 27.21% for the reduced soaking time at austenitizing. The wear rate increases much after double tempering condition onwards indicating material becomes softer, so depending on the hardness required for the application the necessity of further tempering must be decided. The mechanical properties obtained describe its suitability for use in components like intermediate liners in extrusion dies where the hardness requirement is 37- 43HRC.

REFERENCES

- [1] Zheng, Y., Wang, F., Li, C., Lin, Y., and Cao, R. (2019). Effect of Martensite Structure and Carbide Precipitates on Mechanical Properties of Cr-Mo Alloy Steel with Different Cooling Rate. *High Temp. Mater. Process.*, 38, pp. 113-124. DOI:10.1515/htmp-2018-0018.
- [2] Wang, J., Xu, Z. and Lu, X. (2020). Effect of the Quenching and Tempering Temperatures on the Microstructure and Mechanical Properties of H13 Steel. *J. of Materi. Eng. and Perform*, 29, pp. 1849–1859. DOI:10.1007/s11665-020-04686-0.
- [3] Guanghua, Y., Xinmin, H., Yanqing, W., Xingguo, Q., Ming, Y., Zuoming, C., and Kang, J. (2010). Effects of heat treatment on mechanical properties of H13 steel. *Met. Sci. Heat Treat.* 52, pp. 393-395. DOI:10.1007/s11041-010-9288-4.
- [4] Chen, C., Yan, K., Qin, L., Zhang, M., Wang, X., Zou, T., and Hu, Z. (2017). Effect of Heat Treatment on Microstructure and Mechanical Properties of Laser Additively Manufactured AISI H13 Tool Steel. *J. Mater. Eng.* 26. DOI:10.1007/s11665-017-2992-0.
- [5] Karmakar, P. D., Gopinath, M., Nath. A. K. (2019). Effect of tempering on laser remelted AISI H13 tool steel, *Surf. Coat. Technol.* 361, pp. 136-149. DOI: 10.1016/j.surfcoat.2019.01.022.
- [6] Krauss, G., (2017), Tempering of Lath Martensite in Low and Medium Carbon Steels: Assessment and Challenges. *steel research int.*, 88: 1700038. DOI:10.1002/srin.201700038.
- [7] Li, S., Wu, X., Chen, S., Junwan, L. (2016). Wear Resistance of H13 and a New Hot-Work Die Steel at High temperature. *J. of Materi. Eng. and Perform*, 25, pp. 2993–3006. DOI:10.1007/s11665-016-2124-2.
- [8] Zhang, J., Ouyang, X., Zhou, J., Zhang, J. (2018). Study on Microstructure and Mechanical Properties of H13 Tool Steel After Chromium Content Reduction. *J. Materials Reports*, 2 32(8): pp. 1323-1327. DOI: 10.11896/j.issn.1005-023X.2018.08.022.
- [9] Jiang, B., Wu, M., Zhang, M., Zhao, F., Zhao, Z., Liu, Y. (2017). Microstructural characterization, strengthening and toughening mechanisms of a quenched and tempered steel: Effect of heat treatment parameters, *Mater. Sci. and Eng. A*, 707, pp. 306-314. DOI: 10.1016/j.msea.2017.09.062.
- [10] Liu, H., Fu, P., Liu, H., Sun, C., Du, N., Li, D. (2019). Effect of vanadium micro-alloying on the microstructure evolution and mechanical properties of 718H pre-hardened mold steel, *J. Mater. Sci. Technol.*, 35(11), pp. 2526-2536. DOI: 10.1016/j.jmst.2019.04.033.
- [11] Wei, M. X., Wang, S. Q., Wang, L., Cui, X. H., Chen, K. M. (2011). Effect of tempering conditions on wear resistance in various wear mechanisms of H13 steel. *Tribol. Int.*, 44(7–8), pp. 898-905. DOI: 10.1016/j.triboint.2011.03.005.
- [12] Barrau, O., Boher, C., Gras, R., Rezai-Aria, F., (2003). Analysis of the friction and wear behaviour of hot work tool steel for forging. *Wear*, 255(7–12), pp. 1444-1454. DOI:10.1016/S0043-1648(03)00280-1.
- [13] Bahrami, A., Mousavi Anijdan, S. H., Golozar, M. A., Shamanian, M., Varahram, N. (2005). Effects of conventional heat treatment on wear resistance of AISI H13 tool steel. *Wear*, 258 (5–6), pp. 846-851. DOI: 10.1016/j.wear.2004.09.008.



- [14] Jagota, V., Sharma, R. K. (2018). Interpreting H13 steel wear behaviour for austenitizing temperature, tempering time and temperature. *J. Braz. Soc. Mech. Sci. Eng.* 40, 219. DOI:10.1007/s40430-018-1140-6.
- [15] Zhang, M., Li, C., Gao, Q., Fang, J., Li, Wu, T., Wang, Hong, K. (2020). The effect of heat treatment on microstructure and properties of laser-deposited TiC reinforced H13 steel matrix composites, *Optik*, 206, 164286. DOI:10.1016/j.ijleo.2020.164286.
- [16] Wang, X., Wang, J., Gao, Z., Xia, D., Hu, W. (2019). Tempering effects on the microstructure and properties of submerged arc surfacing layers of H13 steel. *J. Mater. Process Technol.*, 269, pp. 26-34. DOI: 10.1016/j.jmatprotec.2019.01.024.
- [17] Galindo-Nava, E. I., and Rivera-Díaz-Del-Castillo, P. E. J. (2016). Understanding the factors controlling the hardness in martensitic steels. *Scripta Materialia*, 110. pp. 96-100. DOI: 10.1016/j.scriptamat.2015.08.010.
- [18] Qamar, S. Z., Sheikh, Arif, A. F., Pervez, T., Siddiqui, R. A., (2007). Heat treatment of a hot-work die steel. *Arch. Mater. Sci. Eng.* 28(8), pp. 503-508.
- [19] Koyama, M., Zhang, Z., Wang, M., Ponge, D., Paabe, D., Tsuzaki, K., Noguchi, H., Tasan, C. C. (2017). Bone-like crack resistance in hierarchical metastable nanolaminate steels. *Science*, 355(1055–1057). DOI:10.1126/science.aal2766.
- [20] Li, S., Guoming Z., Kang, Y. (2017). Effect of substructure on mechanical properties and fracture behavior of lath martensite in 0.1C–1.1Si–1.7Mn steel. *J. Alloys Compd.*, 675, pp. 104-115. DOI: 10.1016/j.jallcom.2016.03.100.
- [21] Wang, M., You, B., Wu, Y., Liang, B., Gao, X., Li, W., Wei, Q. (2022). Effect of Cr, Mo, and V Elements on the Microstructure and Thermal Fatigue Properties of the Chromium Hot-Work Steels Processed by Selective Laser Melting. *Metals*, 12, 735. DOI:10.3390/met12050735.
- [22] Wang, Z., Rahka, K., Nenonen, P., Laird, C. (1985). Changes in morphology and composition of carbides during cyclic deformation at room and elevated temperature and their effect on mechanical properties of Cr-Mo-V steel, *Acta Metallurgica*, 33(12), pp. 2129-2141. DOI:10.1016/0001-6160(85)90174-9.
- [23] Godec, M., Skobir Balantič, D. (2016). Coarsening behaviour of $M_{23}C_6$ carbides in creep-resistant steel exposed to high temperatures. *Sci Rep* 6, 29734. DOI:10.1038/srep29734.
- [24] Ning, A., Mao, W., Chen, X., Guo, H., Wang M. (2017). J. Precipitation Behavior of Carbides in H13 Hot Work Die Steel and Its Strengthening during Tempering. *Metals*, 7, 70. DOI:10.3390/met7030070.
- [25] Oksiuta, Z., Lewandowska, M., Kurzydowski, J. K., Baluc, N. (2013). Effect of vanadium addition on the microstructure and mechanical properties of the ODS ferritic steels, *J. Nucl. Mater.*, 442(1–3), pp. S84-S88. DOI: 10.1016/j.jnucmat.2012.10.022.
- [26] Shinde, T. (2021) Influence of carbide particle size on the wear performance of cryogenically treated H13 die steel, *Surf. Eng.*, 37(9), pp. 1206-1214. DOI:10.1080/02670844.2019.1701858.
- [27] Özer, M. (2022). Influence of heat treatments on microstructure and wear behaviour of AISI H13 tool steel. *Kovove Materialy*, 60, pp. 387-396. DOI:10.31577/km.2022.6.387.
- [28] Xie, Y., Cheng, X., Wei, J., Luo, R. (2022). Characterization of Carbide Precipitation during Tempering for Quenched Dievar Steel. *Materials* 15, 6448. DOI:10.3390/ma15186448.
- [29] Saha, A., Jung, J. and Olson, G.B. (2007). Prototype evaluation of transformation toughened blast resistant naval hull steels: Part II. *J. Computer-Aided Mater Des*14, 201–233. DOI:10.1007/s10820-006-9032-y.
- [30] Wang, Y., Song, K., Zhang, Y., Wang, X. (2019). Microstructure evolution and fracture mechanism of H13 steel during high temperature tensile deformation, *Mater. Sci. Eng. A*, 746, pp. 127-133. DOI: 10.1016/j.msea.2019.01.027.
- [31] Zhou, J., Dang-shen, M. A., Chi, H., Chen, Z., Li, X., (2013) Microstructure and Properties of Hot Working Die Steel H13MOD, *J. Iron Steel Res. Int.*, 20(9), pp. 117-125. DOI:10.1016/S1006-706X(13)60166-1.
- [32] Bhadesia, H., and Honeycombe, R. (2017). *Steels microstructures and properties*. Fourth edition. DOI: 10.1016/B978-0-08-100270-4.00005-6.
- [33] Virtanen, E., Van Tyne, C. J., Levy, B. S., Brada, G. (2013). The tempering parameter for evaluating softening of hot and warm forging die steels, *J. Mater. Process. Technol.* 213(8), pp. 1364-1369. DOI: 10.1016/j.jmatprotec.2013.03.003.